NANO LETTERS

Letter

pubs.acs.org/NanoLett

Buried Nanoantenna Arrays: Versatile Antireflection Coating

Ali Kabiri,[†] Emad Girgis,[†,‡] and Federico Capasso*[,†]

[†]School of Engineering and Applied Sciences (SEAS), Harvard University, Mckay Gordon Building, Capasso Lab, Room 125, Cambridge, Massachusetts 02138, United States

[‡]Solid State Physics Department, National Research Centre, El-Behouth Street, Dokki, Giza, Egypt

Supporting Information

ABSTRACT: Reflection is usually a detrimental phenomenon in many applications such as flat-panel-displays, solar cells, photodetectors, infrared sensors, and lenses. Thus far, to control and suppress the reflection from a substrate, numerous techniques including dielectric interference coatings, surface texturing, adiabatic index matching, and scattering from plasmonic nanoparticles have been investigated. A new technique is demonstrated to manage and suppress reflection from lossless and lossy substrates. It provides a wider flexibility in design versus previous methods. Reflection from a surface can be suppressed over a narrowband, wideband, or multiband frequency range. The antireflection can be dependent or independent of the incident wave polarization. Moreover, antireflection at a very wide incidence angle can be attained. The reflection from a substrate is controlled by a buried nanoantenna array, a structure composed of (1) a subwavelength metallic array and (2) a dielectric cover layer referred to as a superstrate. The material properties and thickness of the superstrate and nanoantennas' geometry and periodicity control the phase and intensity of the wave circulating inside the superstrate cavity. A minimum reflectance of 0.02% is achieved in various experiments in the mid-infrared from a silicon substrate. The design can be integrated in straightforward way in optical devices. The proposed structure is a versatile AR coating to optically impedance matches any substrate to free space in selected any narrow and broadband spectral response across the entire visible and infrared spectrum.

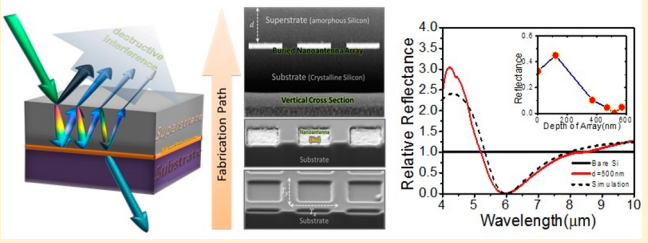

KEYWORDS: *Buried nanoantenna array, plasmonic antireflection coating, plasmonic matching layer, plasmonic filters, metasurfaces, Smith Chart*

Optical nanoantennas are an enabling technology for manipulating and controlling light at nanometer scale.[1] Analogous to microwave antennas, they convert radiative energy into localized energy. Photons coupled into metallic nanoantennas excite plasmons, collective oscillations of free electrons in metal. The entire response of a nanoantenna array can be tuned by the nanoantennas' geometry and periodicity. Nanoantenna arrays with optimized optical response have a wide range of applications in optical beam manipulation, energy harvesting, sensing, nonlinear optics and even medical therapies. However, due to the impedance mismatch between the interfacing medium (usually air) and the array patterned on the surface these applications suffer from low performance and inefficiency. Covering the nanoantenna array with a dielectric material of appropriate thickness introduces an additional degree of freedom in controlling light with higher flexibility and desirable efficiency. The ultrathin dielectric cavity above the nanoantenna array is used as a matching layer to the array, and it can enhance the performance of the array. Figure 1A shows the schematic of a buried nanoantenna array, a structure composed of embedded metallic nanoantennas in a substrate covered with a dielectric layer, and Figure 1B–D shows a perspective view and vertical cross-section of the proposed structure in the process of fabrication. The cover layer, called superstrate, can be a lossless or lossy material. The proposed structure can be optimized and integrated into a variety of applications such as solar cells, photo detectors, biosensors and plasmonic planar lenses to enhance efficiency and performance. In this work, we examine antireflection coating based on buried nanoantenna arrays.

Fresnel reflection is a consequence of electromagnetic wave interaction with a dielectric surface. Undesirable reflections can severely limit the performance of optical devices. Over the years, various methods have been used to minimize undesirable reflections in applications. Conventionally, a dielectric interference coating is used to suppress the reflection from a substrate.[2] The purpose of the AR coating layer is usually to achieve an optimum reflection reduction at a certain frequency and incidence angle. For a normal incidence, $n_C = (n_S)^{1/2}$ and $d = \lambda/4$, where n_C and n_S are the refractive index of the coating layer and substrate, d is the coating thickness, and λ is the wavelength in the coating layer. For example, a single layer of Si_3N_4 reduces light reflection from silicon down to 18% only at visible frequencies.[3] However, due to the unavailability of coating materials with an accurate refractive index at desired

Received: August 31, 2013
Revised: November 16, 2013
Published: November 22, 2013

   dx.doi.org/10.1021/nl403257a | *Nano Lett.* 2013, 13, 6040–6047

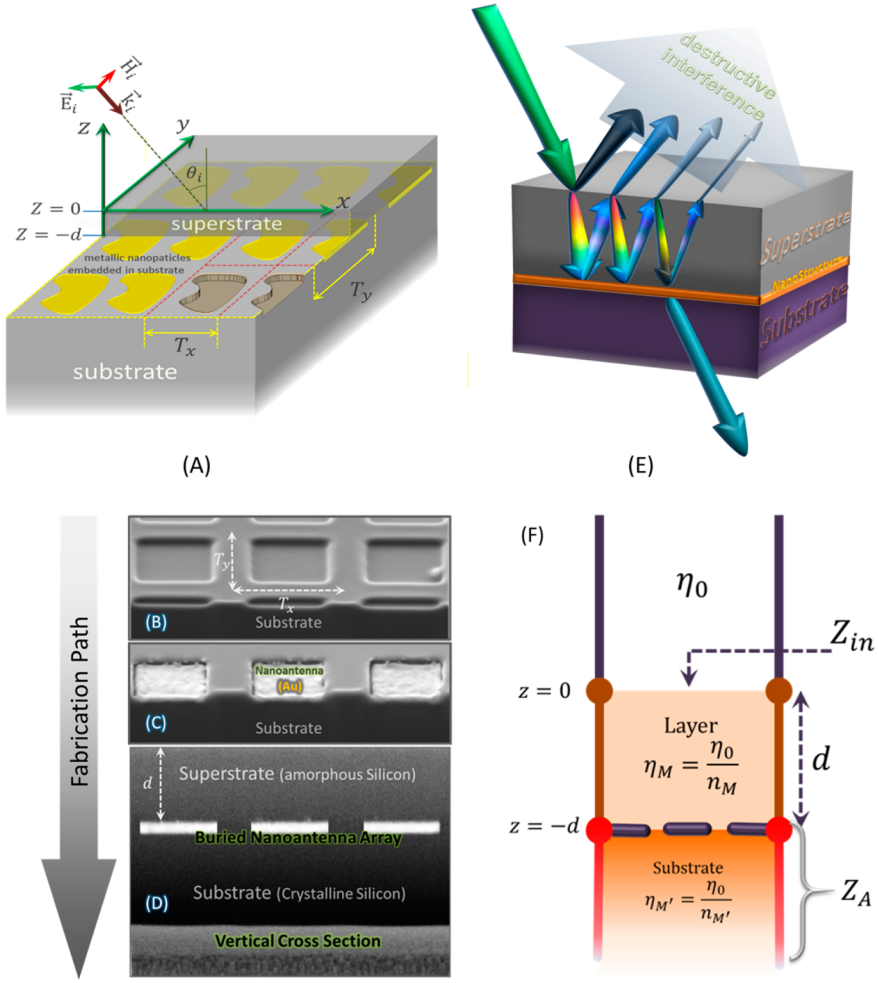

Figure 1. (A) Schematic of buried metallic nanoantenna array. (B–D) Perspective and vertical cross section view of a typical fabricated sample imaged using FIB. (E) Schematic of antireflection mechanism. Reflected waves from the structure destructively interfere to mimic an antireflection coating. The cover layer thickness and the nanoantennas geometry control the appropriate phase and amplitude of the reflected waves (The phase is coded by the color and the amplitude is coded by the thickness of arrows). (F) Schematic of a transmission line model of a buried nanoantenna array. The substrate and metallic nanoantennas are modeled by the impedance Z_A. The cover layer (superstrate) is modeled by a transmission line with a length d and intrinsic impedance η_M (η_M can be a complex number). Z_{in} is the input impedance of the structure observed from free space. The reflectance is minimum if $Z_{in} = \eta_0$ (impedance matching condition).

frequencies ideal reflection suppression is unachievable. Multilayer AR coatings have also been proposed to reduce the reflectance of a single layer AR coating.[4] For example, a double layer coating of ThF_4 and ZnSe reduces reflection from a CO_2 laser up to 10% on average at mid-infrared frequencies.[5] Commercial multilayer AR coatings are used to reduce the reflectance from a substrate to less than 1% over a desired frequency band. However, integration of multilayer AR coatings in photonic chips is quite challenging.

Micron- and submicrometer-sized surface texturing is an alternative technique that is mainly used for solar cell applications to trap light at the interface of the dielectric substrate; it eliminates reflection and enhances light coupling efficiency.[6] Fabrication of aperiodic or periodic arrays of semiconductors with various geometry including nanowires, nanospheres, and nanotips on the surface of a silicon wafer has proven to be a remarkable reflection reduction technique over visible and up to mid-infrared frequencies.[7−10] In surface texturing techniques, the optimized properties are achieved through multiple scattering of light which cause wideband reflection reduction. In addition, the adiabatic light coupling to the structure with the refractive index gradient creates a wide angular response.[11−13] In practice, however, the actual reflection suppression from a textured surface depends on the smoothness of the index profile and on how homogeneous surface roughness is. Therefore, achieving high-quality and precise nanotextured surface fabrications for a desirable antireflection effect is expensive and laborious and thus inappropriate for applications. Moreover, in solar applications surface texturing increases the surface area leading to an increase in minority carrier recombination on the surface and junction regions, which is particularly detrimental to the efficiency of thin-film solar cells.[14]

Plasmonic nanoparticles were recently used in light trapping mainly in solar cell applications over the visible spectrum to enhance the performance of photovoltaic devices.[14−17] On average, forming randomly dispersed self-assembled metallic nanoparticles over silicon-on-insulator solar cells shows a 30% increase in photocurrent over the solar spectrum.[16] Numerous studies have investigated the effects of shape, size, array pitch, and material as well as the dielectric spacers in solar cell applications.[15,16] Reflection reduction is achieved as a result of

dx.doi.org/10.1021/nl403257a | Nano Lett. 2013, 13, 6040−6047

the plasmonic resonance and preferential forward scattering mediated by nanoparticles.[17−19] Indeed, metal nanoparticles provide additional advantages such as an enhanced optical path length as a result of angular redistribution of light inside the substrate, light trapping in thin-film dielectric substrates by coupling to waveguide modes, and strong interparticle coupling due to proximity of nanoparticles.[19] These effects directly impact the efficiency of solar cells. It has been shown that spheroidal, hemispherical, and cylindrical silver nanoparticles on a Si_3N_4 spacer layer provide maximum light scattering into the substrate. Experimental data demonstrate an 8% enhancement over any conventional AR coating.[14] Dielectric coatings were also used as an over layer to further tune the performance.[20] However, the performance is highly limited by the thickness, roughness, and dielectric properties of the coatings.

In this work, the properties of buried nanoantenna arrays as an AR coating are investigated. A buried nanoantenna array is used as a tailoring layer to match any substrate to free space. The tailoring structure is composed of two parts: the array of subwavelength metallic inclusions embedded in the substrate and a dielectric cover layer (superstrate). The structure is a modified asymmetric Fabry−Perot cavity with one reflecting side comprising a plasmonic structure embedded in a dielectric substrate.

The proposed technique extends the use of plasmonic structures as a matching layer for any application demanding maximum light coupling. It can be applied to wave reflection reduction from low loss, high loss, and gain materials at all frequencies. It has major advantages compared to the previous antireflection techniques. The wave reflection from a material can be suppressed over narrow and wide band as well as a multiband frequency. The reflection suppression can be made dependent or independent of the incident wave polarization. Moreover, antireflection at a very wide incidence angle can be attained. For example, the performance of dual band forward looking infrared (FLIR) imagers can be enhanced by increasing the simultaneous throughput of both sensor bands in optical systems.[21] Because a conventional single-layer AR coating optimizes the performance for one of the spectral bands, a multilayer dual-band infrared AR coating is used to optimize the response for the midwavelength infrared (MWIR) (3.5 to 5 μm) and far-wavelength infrared (FWIR) (7.8 to 10.5 μm) spectral bands simultaneously. These designs are thicker, more complicated, and costlier. However, antireflection techniques incorporating plasmonic layers can be tuned perfectly to exhibit antireflection for both frequency bands by design of nanoantennas without increasing the thickness.

The technique is not limited to certain dielectric properties of materials. Thus, reflection from any dielectric substrate at any frequency can be suppressed. Unlike conventional AR coatings, by using the proposed technique the reflection can be also suppressed from highly lossy substrates. Such a property has not been achieved through previous techniques. In addition, although materials with a very low refractive index such as fused silica (n = 1.45 @ 1 μm) are almost transparent, their surfaces still reflect a minimum of about 5% of the incident wave. No conventional AR coatings are available for such materials but the proposed structure offers a design to suppress reflection from low contrast dielectric layers. It can be also integrated in optical, infrared, and terahertz applications. Metal loss in the infrared and visible frequency band contributes to the absorption of energy by plasmonic elements. Although this effect does not have any impact on reflection suppression, it reduces the transmittance ratio of the structure. Indeed, this effect could be beneficial in the design of highly absorptive structures applicable in infrared detectors and infrared energy-harvesting rectifiers. Similar methods of absorption enhancement have recently been proposed and demonstrated for use in tunable infrared absorbers.[22,23]

Theory. Figure 1A shows the schematic of a dielectric substrate and a buried nanoantenna array located at $z \leq 0$ with the free space interface at $z = 0$. The nanoantenna array is located at the $z = -d$ plane. The periodicity of elements in x- and y-directions are T_x and T_y, respectively. The incident electromagnetic beam makes an angle θ with the normal direction (z-axis) to the superstrate.

The antireflection mechanism is based on the destructive interference of all rays reflected from the structure. The rays are generated in the multipath circulation of the wave inside the superstrate cavity (see Figure 1E). In the figure, arrows indicate partial waves. They are color coded to show the wave phase change and thinned to show wave intensity change. In each round trip, the wave phase and intensity are changed by (i) propagation of light in the superstrate and (ii) the interaction of light with the buried nanoantenna array. The superstrate thickness only affects the wave phase if it is optically transparent. In addition, the wave interacts with the buried array and drives the nanoantennas to resonate at a certain frequency. The nanoantennas' resonant frequency is determined by their geometry and materials as well as by the host material. The wave phase is abruptly shifted according to the resonant characteristics of the nanoantennas and the wave intensity is changed according to the array scattering efficiency. In order to completely suppress reflection, the partial wave phase and intensity must appropriately be tuned by the superstrate and buried nanoantennas.

To study a buried nanoantenna array, a transmission line (TL) theory is adopted. Figure 1F shows an equivalent TL model for the structure demonstrated in Figure 1A. Without any loss of generality, the propagation direction is considered normal to the structure. In Figure 1F, the impedance of the nanoantenna array, patterned at $z = -d$ on the substrate of refractive index $n_{M'}$, is modeled by $Z_A = R_A + jX_A = R_A + j(\omega L_A - (1/\omega C_A))$, where R_A, X_A, L_A, and C_A are resistance, reactance, inductance, and capacitance of the nanoantenna array, respectively, and $j = (-1)^{1/2}$. At $\omega_r = (L_A C_A)^{-1/2}$, Z_A is purely resistive, for $\omega < \omega_r$ X_A is positive and the nanoantenna array is inductive, and for $\omega > \omega_r$ X_A is negative and the nanoantenna array is capacitive. The superstrate is modeled by a transmission line with an intrinsic impedance $\eta_M = \eta_0/n_M$ where $\eta_0 = (\mu_0/\varepsilon_0)^{1/2}$ is the free space impedance, and n_M is the refractive index of the superstrate with a thickness of d. In order to eliminate the reflection, the impedance matching condition $Z_{in} = \eta_0$, where Z_{in} is the structure impedance measured from free space, must be satisfied. According to the TL theory[23]

$$Z_{in} = \eta_M \frac{Z_A + j\eta_M \tan(kd)}{\eta_M + jZ_A \tan(kd)} \quad (1)$$

where k is the wave vector in the superstrate. Using[1] and the impedance matching condition, the normalized nanoantenna impedance is obtained as

$$\zeta_A = r_A + jx_A = \frac{n_M - j\tan kd}{1 - jn_M \tan kd} \quad (2)$$

dx.doi.org/10.1021/nl403257a | Nano Lett. 2013, 13, 6040−6047

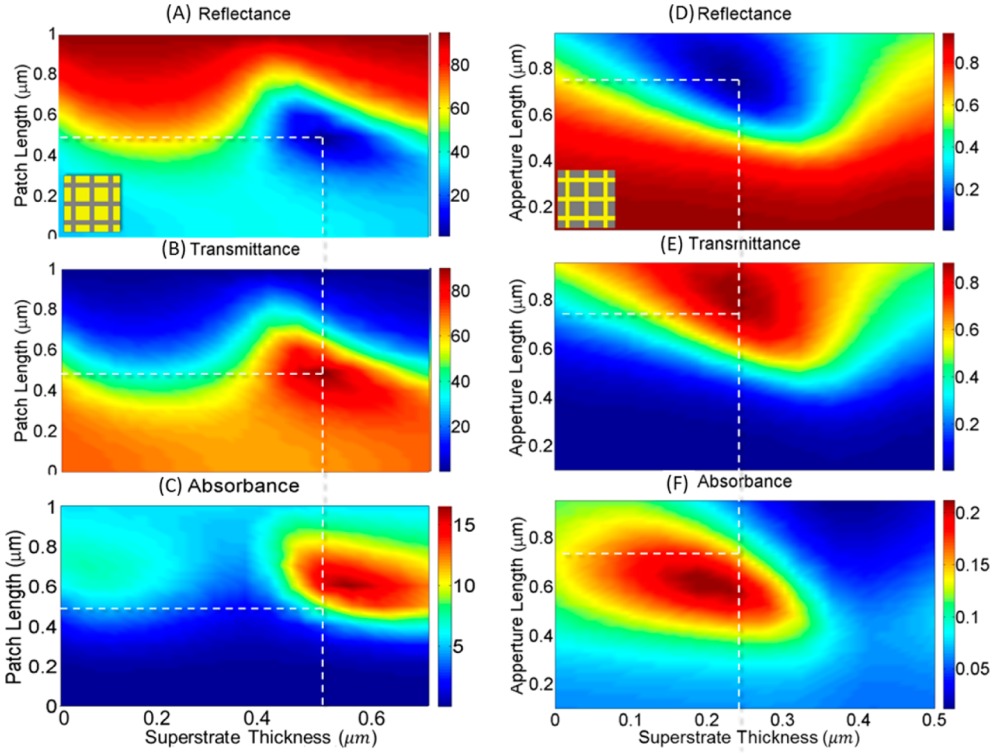

Figure 2. Numerical results for propagation of light at wavelength $\lambda = 6$ μm, through nanoantenna arrays (with $T_x = T_y = 1$ μm) embedded in a silicon substrate and buried under an amorphous silicon superstrate. Reflectance is mapped by color. The color map ranges from dark red for the highest values to dark blue for the lowest values. The dashed lines intercept at the minimum reflectance and maximum transmittance, and they show the superstrate thickness and nanoantenna length for optimum design. (a–c) Reflectance, transmittance, and absorbance for a buried square patch nanoantenna array shown in the left down corner of (a), respectively. Yellow-colored squares are patch nanoantennas on a silicon substrate. Reflectance is plotted versus the patch size (y-axis) and superstrate thickness (x-axis). A design with patch size of about 500 nm and at the depth of about 520 nm = 0.32λ (larger than a quarter of wavelength as the patch nanoantenna array shows capacitive response where $\zeta_A = 0.33 - j0.43$) exhibits antireflection property. (d–f) are reflectance, transmittance, and absorbance for a buried square aperture nanoantenna array shown in the left down corner of (d), respectively. The gray squares are apertures in gold film. The power intensities plotted versus the aperture size and superstrate thickness. A design with patch size of about 760 nm and at the depth of about 240 nm = 0.14λ (smaller than a quarter of wavelength as the aperture nanoantenna array shows capacitive response, where $\zeta_A = 0.41 + j0.68$) exhibits antireflection property.

where $\zeta_A = Z_A/\eta_M$ is the intrinsic impedance of the substrate with refractive index $n_{M'}$, and $r_A = R_A/\eta_{M'}$, $x_A = X_A/\eta_{M'}$ and $\eta = \eta_0/n_{M'}$ (see Supporting Information for detailed calculation).[24] Equation 2 forms a nontrivial relationship between r_A and x_A. Accordingly, a specific pair of (r_A,x_A) satisfies the impedance matching condition. If n_M is given, the pair (r_A,x_A) defines a circle in the impedance complex plane and on the Smith Chart, the reflection coefficient complex plane; that is, the center and radius of the circle are a function of the superstrate refractive index. Each point on the circle corresponds to a superstrate thickness. Since r_A and x_A are dependent, the nanoantenna resistance and reactance must be simultaneously designed in order to achieve reflection suppression. This condition has always been neglected in all designs of solar cell efficiency enhancement using plasmonic nanoparticles.[14−16] (see Supporting Information).

Analytical models for impedance of various antenna geometries can be found in refs 1 and 25−28 and references therein. At infrared and optical frequencies, due to the dielectric-like response of metals both conduction and displacement currents contribute to the nanoantenna impedance. In addition, because in practice the nanoantennas are only a fraction of the infrared and optical wavelength, the phase change in the current distribution is associated with radiation resistance, the equivalent resistance that would dissipate the same amount of power as that radiated from an antenna.[29] Therefore, an accurate estimate of Z_A in the corresponding frequency band is attained by the sum of both material characteristics impedance Z_C and nanoantenna impedance Z_R. Moreover, expressions for these impedances depend on the geometry of nanoantennas. However, the contribution of the radiation resistance is significantly decreased by the reduction of the nanoantenna size compared to the wavelength. In addition, the bandwidth response also depends on ohmic and radiation losses. For example, if the ohmic loss is high, then the nanoantenna quality factor is lower and the bandwidth wider. While the choice of the nanoantenna shape is arbitrary, there are certain factors that must be considered as a guideline (see Supporting Information).

Numerical and Experimental Results. In this report, nanoantennas are made of gold embedded in crystalline silicon (xSi) of refractive index $n_M' = n_{xSi} = 3.4$ and buried under an amorphous silicon (aSi) layer of refractive index $n_M = n_{aSi} = 3.7$ at mid-infrared (mid-IR) wavelengths. The nanoantennas are designed to operate at a center free space wavelength of $\lambda_0 = 6$ μm. The wavelength in amorphous silicon is $\lambda_{aSi} = 1.62$ μm; thus, $d < \lambda_{aSI}/4 = 405$ nm for an inductive nanoantenna array and $d > 405$ nm for a capacitive nanoantenna array. Square patch and square aperture nanoantennas are considered as candidates for capacitive and inductive nanoantenna arrays,

dx.doi.org/10.1021/nl403257a | Nano Lett. 2013, 13, 6040−6047

respectively.[25,26] The propagation of an electromagnetic wave through square patch and aperture nanoantenna arrays embedded in a silicon substrate and buried under amorphous silicon superstrate has been calculated numerically. The reflectance, transmittance, and absorbance are plotted versus nanoantenna size and superstrate thickness in Figure 2.

The input impedance Z_{in} is a function of nanoantenna dimensions, array periodicity, superstrate thickness, and material, as well as the substrate material. According to the impedance matching condition, $Z_{in} = \eta_0$ is a purely real value where the zero reflection occurs ($X_{in} = 0, Z_{in} = R_{in}$). R_{in} is a combination of ohmic resistance and radiation resistance. In general, the maximum of ohmic resistance does not necessarily occur where the impedance matching condition is satisfied. For example, for the patch nanoantenna array the maximum absorbance is blueshifted with respect to the minimum reflectance because the radiation resistance increases as the nanoantenna size approaches half of a wavelength.

Buried nanoantenna arrays with different nanoantenna geometries including the square rod, square and rectangular patch, circular disk, and square aperture have been designed, fabricated, and tested in order to demonstrate reflection suppression from a silicon substrate. In all designs, primarily a TL model was used to estimate the required impedance and superstrate thickness. Then, based on the analytical expression available in the literature, initial dimensions for nanoantennas with specific geometry were calculated. Next, a 3D full-wave EM simulator is used to verify the theory as well as to optimize different geometries in order to achieve reflection suppression. The buried nanoantenna array is fabricated in three major steps. First, the material surface is engraved with specific pattern. Second, the pattern is filled with gold to form the nanoantenna array. Third, a dielectric material with a specific thickness is deposited on top of the matrix of elements to form a buried nanoantenna array. Fourier transform infrared (FTIR) spectroscopy is used to measure reflectance from the sample.

Figure 3A–C shows the measurement results and SEM images of buried nanoantenna arrays composed of square patches, circular disks, and square apertures in four layers in different stages of fabrication. Layers are the following: L1, engraved crystalline silicon substrate; L2, the engraved structure filled with gold layer (embedded nanoantennas); L3, nanoantenna array buried under 100 nm thick amorphous silicon; and L4, nanoantenna array buried under 500 nm thick amorphous silicon. On the right side of each SEM image, the corresponding spectral reflectance curves of samples for different superstrate thicknesses are plotted. The experimental data were compared with the optimized simulation results as well as the reflectance of AR-coated silicon using Si_3N_4. The simulated and measured results are in good agreement. All structures exhibit a minimum reflectance of less than 1% at λ = 6 μm for different bandwidths. Also, the minimum reflectance for different superstrate thickness is plotted versus the superstrate thickness (small window graphs). As it is expected, the minimum reflectance is achieved for superstrate thickness larger than quarter wavelength (405 nm) for designs based on square patch and circular disk nanoantenna arrays because these exhibit capacitive responses, and less than quarter wavelength (405 nm) for the design based on square aperture since these exhibit inductive responses. Because the metallic structure is used in design of AR coating, part of the energy is dissipated in metal. However, the transmittance can be achieved as high as 95%. Figure 3D shows transmittance of structures

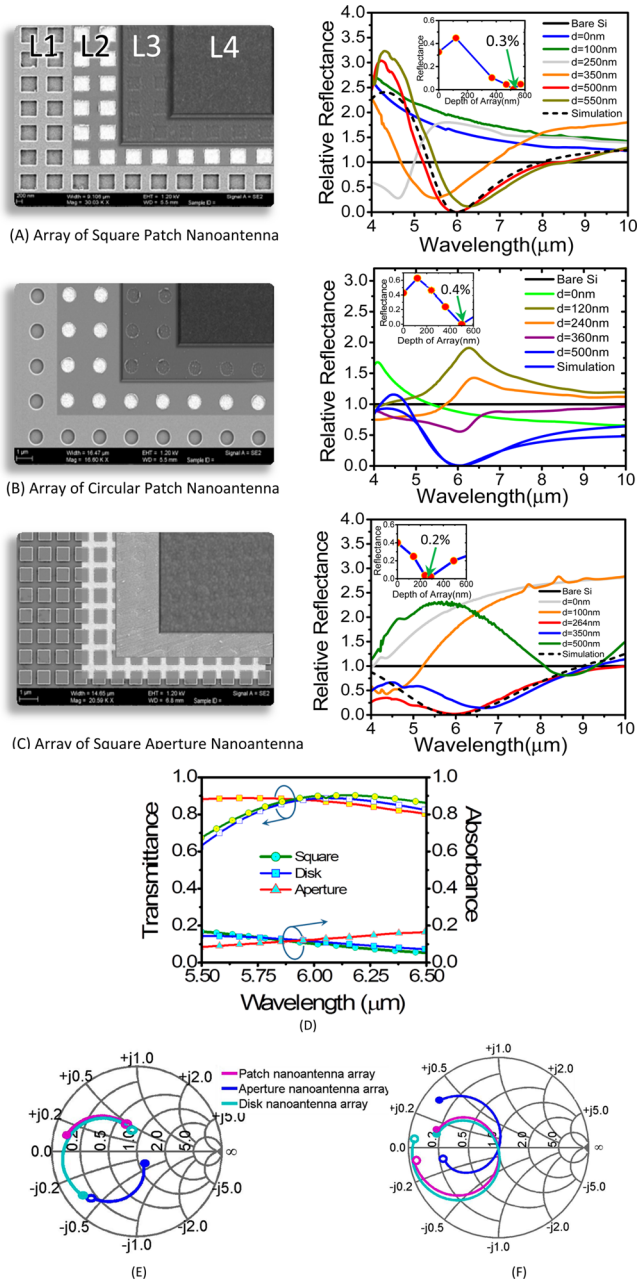

Figure 3. SEM images and measured reflectance for different structures. SEM images demonstrate the following four layers. L1, patterned substrate, L2, embedded nanoantennas, L3, covered amorphous silicon layer (100 nm), and L4, covered amorphous silicon (500 nm) (marked in A). The plots show the relative reflectance from a crystalline silicon substrate patterned with (A) square nanoantennas, (B) disk nanoantennas, (C) aperture nanoantennas, and covered with amorphous silicon (superstrate) with different thicknesses. The plots are normalized to the measured reflectance of bare crystalline silicon of the same wafer. The inset shows the absolute reflectance versus the superstrate thickness for different nanoantenna geometries at λ = 6 μm. The absolute reflectance is calculated by multiplying the relative reflectance and reflectance of crystalline silicon (= 0.30). A minimum reflectance of 2.6 × 10^{-3}, 4.1 × 10^{-3}, and 1.6 × 10^{-3} is achieved for designs based on patch, disk, and aperture nanoantenna arrays, respectively. (D) Transmittance and absorbance of the three structures in panels A–C. For reflectance measurement single-side polished crystalline silicon substrate and for transmittance measurement double-side polished crystalline silicon substrates are used. (E) The normalized impedance,

dx.doi.org/10.1021/nl403257a | Nano Lett. 2013, 13, 6040–6047

Figure 3. continued

ζ_A, of the nanoantenna arrays patterned on the silicon substrate. (F) The normalized input impedance, Z_{in}, of the structure. The open dots and closed dots on the Smith Charts correspond to $\lambda = 4$ μm and $\lambda = 10$ μm. Panel E shows an inductive response of aperture nanoantenna array and capacitive response of patch nanoantenna array. In panel F, all impedance curves intercept at the origin at $\lambda = 6$ μm representing that the structures are matched with free space, and reflection is minimized.

designed with buried disk, patch, and aperture nanoantenna array demonstrated in Figure 3A–C. (Also see Figure 4F for absorption of different size buried patch nanoantenna array.) Figure 3E,F shows the normalized input impedance of the structure before and after deposition of superstrate. Figure 3F shows matching of structures in Figure 3A–C with free space.

In Figure 4A, the frequency bands through which the reflection has been suppressed were compared for the different nanoantenna geometries. The study shows that a buried rod-shaped nanoantenna array leads to the narrowest reflection suppression response while a buried aperture nanoantenna array, and a multisquare patch and aperture nanoantenna array form the widest reflection suppression. The bandwidth of each structure can be independently calculated based on the values of equivalent capacitance, inductance, and resistance of the array. In addition, unlike patch and circular shape nanoantenna geometries, rod-shaped nanoantenna geometry provides polarization dependent reflection suppression. The reflection of the wave with the electric field along the rod is suppressed while of the wave with perpendicular polarization is completely reflected. Thus, unidirectional and omnidirectional antireflection can be achieved. This property is not achievable with conventional single or multilayer AR coatings.

Figure 4B shows the reflectance of antireflection coating designs based on patch nanoantenna arrays with different array periodicities. If the buried nanoantenna periodicity is decreased, the nanoantennas' size is decreased. If the nanoantennas' size is much smaller than half a wavelength, they exhibit a non-radiative quasi-static response. Metallic elements at close proximity of each other are coupled and form a network of lumped circuit elements comprising inductors and capacitors. The circuit network of inductance L and capacitance C resonates at the resonant frequency of $1/(LC)^{1/2}$ behaving as a filter. The Q-factor of the resonance depends on the equivalent ohmic resistance per unit square area of nanoantennas. The nanoantennas are made of gold metals; thus, the ohmic loss is directly proportional to the unit area of nanoantenna array. Therefore, by decreasing the array periodicity the absorption is decreased while the bandwidth is increased. This behavior is shown in Figure 4C, and the metamaterial region is highlighted in blue in the figure.

Alternatively, if the nanoantenna dimensions are comparable to half a wavelength of the incident wave, the current distribution induced by an electric field has a nonuniform phase distribution that leads to high radiative fields. Also, the

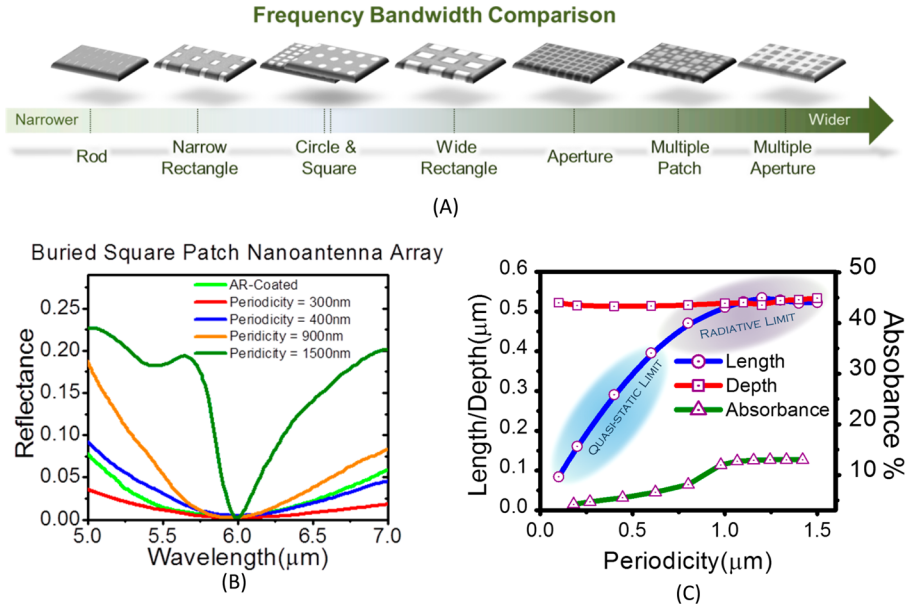

Figure 4. (A) Summary of reflectance of buried nanoantenna arrays with different nanoantennas' geometry (rod, circular disk, narrow and wide rectangular patch, single and multisquare patch, multisquare patch, single and multisquare aperture). A buried rod-shaped nanoantenna array shows the sharpest antireflection response, while multisquare patch and aperture nanoantenna array give the broadest band reflection suppression. (B) Reflectance comparison between antireflection coating designs using buried patch nanoantenna arrays with different periodicity and a silicon substrate coated with a quarter wavelength of Si_3N_4. Arrays with larger periodicity show sharper spectral reflectance response; therefore, they can be used as a narrow band-pass or notch filters. Arrays with smaller periodicity exhibit broadband reflection suppression. Buried nanoantenna arrays with periodicity of 400 nm and less show broader band reflection suppression in comparison with conventional single layer AR coatings. (C) Length, depth, and absorbance of various AR coating structures versus the array periodicity. The AR coating is designed at $\lambda = 6$ μm. The nanoantennas are located at about 500 nm depth for all designs. That is, the nanoantenna arrays have similar impedance. Therefore, nanoantennas with larger size show strong resonating behavior (highlighted in purple), and nanoantennas with smaller length operate in the quasistatic limit (highlighted in blue), and they create a capacitive network. Consequently, the absorption changes nonlinearly with periodicity. At larger periodicity, the absorption remains constant as the size of nanoantennas remains constant, while at smaller periodicity the absorption reduces in proportion to the relative ratio of the nanoantenna area to the unit cell area, and it approaches a constant value.

dx.doi.org/10.1021/nl403257a | *Nano Lett.* 2013, 13, 6040–6047

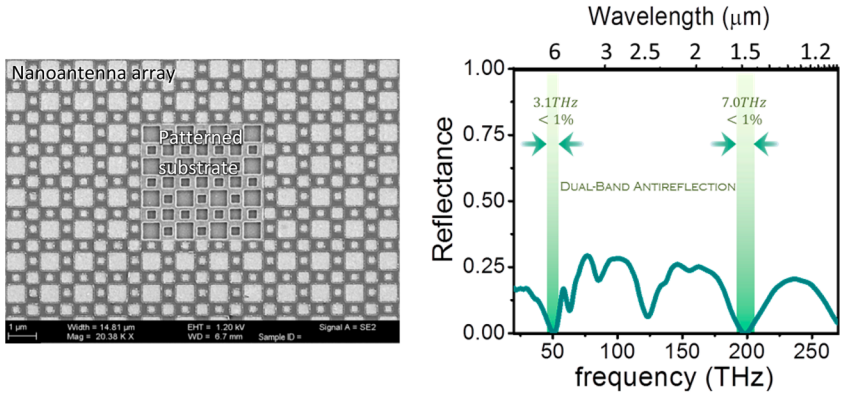

(A) (B)

Figure 5. Dual-band antireflection response formed by buried multisquare patch nanoantenna array. (A) SEM image of multisquare patch nanoantennas. The image shows a patterned substrate and embedded nanoantennas. (B) The experimental result shows two bands of antireflection response at 50 THz (6 μm) and 200 THz (1.5 μm) with a bandwidth of about 7 THz, less than 1% relative bandwidth in both bands.

maximum field absorption occurs at resonance. At resonance, the reactance of the nanoantenna array becomes zero and the impedance becomes purely real. The nanoantenna input resistance is a combination of radiation and ohmic resistance. Since the nanoantenna geometry and size determine the nanoantenna resonance, array periodicity variation does not change this condition. Thus, the absorption remains constant as the periodicity increases. The region corresponding to the large size nanoantenna has been highlighted in purple in Figure 4C. The figure also shows that variation of the periodicity and nanoantenna size has no effect on the superstrate thickness because the thickness of the superstrate is determined by the impedance of the nanoantenna array, and in all cases the nanoantenna input impedance can be kept constant.

As it has already been discussed, many applications such as FLIR imagers demand multiple band antireflective response. Structures with multiresonance responses can be designed to suppress reflected beam in multiple bands. A simple structure of multiple patches has been optimized to eliminate the reflected infrared beam from a silicon substrate at near-IR λ_1 = 2 μm and mid-infrared λ_2 = 6 μm. Figure 5 shows the SEM image and measurement results for dual-band antireflection based on buried nanoantenna arrays. Evidently, if in the design of multisquare patch, the eliminated frequencies of consecutive bands are designed appropriately, ultrawide antireflection can be achieved.

Although the plasmonic nanoantennas are mainly insensitive to the incidence angle, there is another mechanism that controls the incidence angle dependence of the reflectance. Reflection suppression can be achieved for waves at wide incidence angles by selecting a high contrast cover layer (see Supporting Information).

Simulations. All structures are simulated using Computer System Technology Studio Suite version 2013, a commercial three-dimensional electromagnetic full wave simulator.

Measurement Setup and Fabrication. The buried nanoantenna samples are fabricated on a polycrystalline silicon 2 in. wafer substrate with standard electron-beam lithography (Elionix-125) and positive double layers resist (PMMA495/950). After developing the e-beam resist, the Si samples were etched using reactive ion etching (RIE), subsequent deposition of 1 nmTi/50 nmAu, and lift-off processes. The samples were investigated using high-resolution SEM (SEM8 FESEM ultra plus) and focused ion beam (FIB/SEM). Also, Figure 1B shows the steps of fabrication process. The reflection and transmission were measured in the mid infrared range using an FTIR spectrometer equipped with a mid-IR microscope (Bruker Vertex 70 FTIR/Hyperion 2000) for focusing.

Conclusion. Recently, plasmonic nanoparticles were introduced as a complement to conventional AR coatings to improve the antireflection effect. However, the limitations of the conventional AR coating such as unavailability of coating materials were inherited in AR techniques involved plasmonic nanoparticles. In this work, we introduced new technique to suppress reflection, which does not suffer from limitations of previous techniques. Instead, it is benefited from advantages of using plasmonic structures such as enhanced optical trapping and wide incidence angle response.

It is shown that the reflected wave is eliminated entirely by fabricating a designed buried nanoantenna array on the substrate. A buried nanoantenna array is a structure composed of a matrix of plasmonic nanoantennas embedded in a substrate and a dielectric cover layer (superstrate).

This technique has several advantages compared to previous techniques. The antireflection can be achieved for any materials as opposed to conventional AR coating which requires a specific coating material with a quarter of wavelength thickness. The proposed technique enables design of antireflection coating with wide or narrow or a multiple frequency band. In addition, reflection suppression can be sensitive or insensitive to polarization and the angle of incident wave.

To suppress reflection, buried nanoantenna arrays with various nanoantenna geometries were designed and experimentally tested. A minimum reflectance of less than 1% was achieved in all experiment. However, each design exhibited different features of suppressed reflected wave.

■ ASSOCIATED CONTENT

Supporting Information

Further details of the theory and the use of the Smith Chart in the design of the buried nanoantenna arrays. Additionally, the theory for design of AR coating with a superstrate with complex refractive index and simulation and experimental data on reflection suppression at oblique incidence. This material is available free of charge via the Internet at http://pubs.acs.org.

dx.doi.org/10.1021/nl403257a | Nano Lett. 2013, 13, 6040−6047

AUTHOR INFORMATION

Corresponding Author

*E-mail: capasso@harvard.edu.

Notes

The authors declare no competing financial interest.

ACKNOWLEDGMENTS

We acknowledge partial financial support from the Air Force Office of Scientific Research (AFOSR) under Contract FA9550-09-1-0505. This work was also financially supported in part by the Natural Sciences and Engineering Research Council of Canada (NSERC) under Postdoctoral Fellowship Program No. PDF-145627234 and also the Fulbright program of Egypt.

REFERENCES

(1) Agio, M.; Alu, A. *Optical Antennas*; Cambridge University Press: New York, 2013.

(2) Fowles, G. R. *Introduction to Modern Optics*; Dover: Mineola, NY, 1975.

(3) Chhajed, S.; Schubert, M. F.; Kim, J. K.; Schubert, E. F. Nanostructured Multilayer Graded-index Antireflection Coating for Si Solar Cells with Broadband and Omnidirectional Characteristics. *Appl. Phys. Lett.* **2008**, *93*, 251108−251110.

(4) Gerecht, E.; Musante, C. F.; Zhuang, Y.; Yngvesson, K. S.; Goyette, T.; Dickinson, J.; Waldman, J.; Yagoubov, P. A.; Gol'tsman, G. N.; Voronov, B. M.; Gershenzon, E. M. NbN hot electron bolometric mixers—A new technology for low-noise THz receivers. *IEEE Trans. Microwave Theory Tech.* **1999**, *47*, 2519−2527.

(5) Harris, D. C. *Materials for Infrared Windows and Domes: Properties and Performance*; SPIE Press Book: Bellingham, WA, 1999.

(6) Southwell, W. H. Pyramid-array surface-relief structures producing antireflection index matching on optical surfaces. *J. Opt. Soc. Am.* **1991**, *8*, 549−553.

(7) Clapham, P. B.; Hutley, M. C. Reduction of lens reflection by the "Moth Eye" principle. *Nature* **1973**, *244*, 281−282.

(8) Xi, J. Q.; et al. Optical thin-film materials with low refractive index for broadband elimination of Fresnel reflection. *Nat. Photonics* **2007**, *1*, 176−179.

(9) Branz, H. M.; et al. Nanostructured black silicon and the optical reflectance of graded-density surfaces. *Appl. Phys. Lett.* **2009**, *94*, 231121−231123.

(10) Huang, Y.; Chattopadhyay, S.; Jen, Y.; Peng, C.; Liu, T.; Hsu, Y.; Pan, C.; Lo, H.; Hsu, C.; Chang, Y.; Lee, C.; Chen, K.; Chen, L. Improved broadband and quasi-omnidirectional anti-reflection properties with biomimetic silicon nanostructures. *Nat. Nanotechnol.* **2007**, *2*, 770−774.

(11) Zhu, J.; Hsu, C. M..; Yu, Z.; Fan, S.; Cui, Y. Optical absorption enhancement in amorphous silicon nanowire and nanocone arrays. *Nano Lett.* **2009**, *9*, 279−282.

(12) Southwell, W. H. Gradient-index antireflection coatings. *Opt. Lett.* **1983**, *8*, 584−586.

(13) Spinelli, P.; Verschuuren, M. A.; Polman, A. Broadband omnidirectional antireflection coating based on subwavelength surface Mie resonators. *Nat. Commun.* **2012**, *3*, 1−5.

(14) Catchpolea, K. R.; Polmanb, A. Design principles for particle plasmon enhanced solar cells. *Appl. Phys. Lett.* **2008**, *93*, 191113−191115.

(15) Spinelli, P.; et al. Optical impedance matching using coupled metal nanoparticle arrays. *Nano Lett.* **2011**, *11*, 1760−1765.

(16) Atwater, H. A.; Polman, A. Plasmonics for improved photovoltaic devices. *Nat. Mater.* **2010**, *9*, 205−213.

(17) Pillai, S.; Catchpole, K. R.; Trupke, T.; Green, M. A. Surface plasmon enhanced silicon solar cells. *J. Appl. Phys.* **2007**, *101*, 093105−093112.

(18) Polman, A. Plasmonics Applied. *Science* **2008**, *322*, 868−869.

(19) Ferry, V.; et al. Light trapping in ultrathin plasmonic solar cells. *Opt. Express* **2010**, *18*, A237−A245.

(20) Xu, G.; Tazawa, M.; Jin, P.; Nakao, S.; Yoshimura, K. Wavelength tuning of surface plasmon resonance using dielectric layers on silver island films. *Appl. Phys. Lett.* **2003**, *82*, 3811−3813.

(21) Rahmlow, T. D., Jr.; Wilkinson, J. E. L. S.; Tinker, F. *Dual band antireflection coatings for the infrared*; SPIE Proceedings 6940; SPIE Press Book: Bellingham, WA, 2008.

(22) Kats, M. A.; Blanchard, B.; Genevet, P.; Yang, Z.; Qazilbash, M.; Basov, D. N.; Ramanathan, S.; Capasso, F. Thermal tuning of mid-infrared plasmonic antenna arrays using a phase change material. *Opt. Lett.* **2013**, *38*, 368.

(23) Pozar, D. M. *Microwave Engineering*; John Wiley & Sons Inc.: New York, 1998.

(24) The superstrate can be any lossless, lossy, or gainy medium, as opposed to conventional methods where a quarter wavelength-thick coating layer with a refractive index $n_M = (n_{M'})^{1/2}$ is used for the design of an AR coating.

(25) Mitra, R.; et al. Techniques for Analyzing Frequency Selective Surfaces—A Review. *Proc. IEEE* **1988**, *76*, 1593−1615.

(26) Wu, T. K. *Frequency Selective Surface and Grid Array*; Wiley: New York, 1995.

(27) Munk, B. A. *Frequency Selective Surfaces: Theory and Design*; Wiley: New York, 2000.

(28) Kem, D. J.; Wemer, D. H.; Wilhelm, M. J.; Church, K. H. Genetically Engineered Multiband High-impedance Frequency Selective Surfaces. *Microwave Opt. Technol. Lett.* **2003**, *38*, 400−403.

(29) Peters, D. W. et al. *Transmissive Infrared Frequency Selective Surfaces and Infrared Antennas*: Final Report for LDRD 105749, 1−45 SAND2009−6012 Unlimited Release Printed September 2009; Sandia National Laboratories: Albuquerque, NM, and Livermore, CA, USA; http://prod.sandia.gov/techlib/access-control.cgi/2009/096012.pdf.